Hohmann et al. *EPJ Quantum Technology* (2015) 2:23
DOI 10.1140/epjqt/s40507-015-0036-y

EPJ Quantum Technology
a SpringerOpen Journal

EPJ.org

RESEARCH Open Access

Neutral impurities in a Bose-Einstein condensate for simulation of the Fröhlich-polaron

Michael Hohmann[1*†], Farina Kindermann[1†], Benjamin Gänger[1], Tobias Lausch[1], Daniel Mayer[1,2], Felix Schmidt[1,2] and Artur Widera[1,2]

*Correspondence:
mibauer@rhrk.uni-kl.de
[1]Department of Physics and Research Center OPTIMAS, University of Kaiserslautern, Gottlieb-Daimler-Strasse 47, Kaiserslautern, 67663, Germany
†Equal contributors

Abstract

We present an experimental system to study the Bose polaron by immersion of single, well-controllable neutral Cs impurities into a Rb Bose-Einstein condensate (BEC). We show that, by proper optical traps, independent control over impurity and BEC allows for precision relative positioning of the two sub-systems as well as for dynamical studies and independent read-out. We furthermore estimate that measuring the polaron binding energy of Fröhlich-type Bose polarons in the low and intermediate coupling regime is feasible with our experimental constraints and limitations discussed, and we outline how a parameter regime can be reached to characterize differences between Fröhlich and Bose-polaron in the strong coupling regime.

Keywords: Bose-Einstein condensate; single atom; impurity; Bose polaron; Fröhlich polaron

1 Introduction

The immersion of single, controllable atoms into a Bose-Einstein condensate (BEC) realizes a paradigm of quantum physics - individual quantum objects interacting coherently with a single or few mode bath. This system allows to experimentally address various questions of quantum engineering, including local, non-demolition measurement of a quantum many-body system [1]; cooling of qubits while preserving internal state coherence [2, 3]; or engineering bath-mediated, long-range interaction between two or more impurities [4]. An impurity strongly interacting with the quantum gas will loose its single particle properties and it is rather described in terms of quasi particles, which are known as Bose polarons [5–7]. Particularly for strong interaction, such systems have been predicted to show remarkable properties such as self-trapping [5] or polaron clustering [8]. Recently, the dynamic as well as interaction effects on polaronic phenomena in Bose gases have attracted much interest [9–13]. Experimentally, impurities in BECs have been introduced, for example, as many atoms of different internal state [14, 15], different atomic species [16, 17], as individual ions [18, 19], or electrons [20].

The system we report on here considers a single, neutral impurity in an ultracold gas, where the effect of impurity-impurity interactions, either direct or mediated by the bath, can be neglected. The corresponding Hamiltonian thus reflects an extremely imbalanced

mixture and can be written as [6, 21]

$$\hat{H} = \sum_{\mathbf{k}} \varepsilon_{\mathbf{k}} \hat{a}^{\dagger}_{\mathbf{k}} \hat{a}_{\mathbf{k}} + \frac{1}{2} \sum_{\mathbf{k},\mathbf{k}',\mathbf{q}} V_{\mathrm{BB}}(\mathbf{q}) \hat{a}^{\dagger}_{\mathbf{k}'-\mathbf{q}} \hat{a}^{\dagger}_{\mathbf{k}+\mathbf{q}} \hat{a}_{\mathbf{k}} \hat{a}_{\mathbf{k}'} + \frac{\hat{p}_I^{\,2}}{2m_I} + \sum_{\mathbf{k},\mathbf{q}} V_{\mathrm{IB}}(\mathbf{q}) \hat{\rho}_I(\mathbf{q}) \hat{a}^{\dagger}_{\mathbf{k}-\mathbf{q}} \hat{a}_{\mathbf{k}}. \tag{1}$$

The first row of Eq. (1) represents the BEC part of the Hamiltonian, where $a^{\dagger}_{\mathbf{k}}$ ($a_{\mathbf{k}}$) creates (annihilates) a boson of mass m_B, momentum $\mathbf{k}$, and energy dispersion $\varepsilon_{\mathbf{k}} = \hbar^2 k^2/(2m_B)$. The interaction of bosons within the BEC is given by the contact s-wave interaction with Fourier transform $V_{\mathrm{BB}}(\mathbf{q})$. The impurity atom of momentum $\hat{p}_I$, mass m_I and density $\hat{\rho}_I$ as well as its interaction with the BEC via the potential V_{IB} are described by the second row in Eq. (1).

1.1 The Fröhlich polaron

Originally, the polaron concept was developed for condensed matter systems to describe electrons moving in a crystal lattice. The interaction between a moving electron and lattice of the ion cores forms a propagating quasi-particle called polaron, comprising electron and surrounding phonon cloud. Specifically the effective mass of the polaron as well as its energy could strongly differ from the bare electron's values depending on the interaction with the crystal [22, 23]. In the limit of very small electronic wave vector, the underlying crystal structure can be neglected, and the crystal can be described as a continuously polarizable medium. In this case, the model to describe polarons is the well-known Fröhlich Hamiltonian [24]

$$\hat{H}_p = \frac{\hat{p}_I^{\,2}}{2m_I} + \sum_{\mathbf{k}\neq 0} \hbar\omega_{\mathbf{k}} \hat{b}^{\dagger}_{\mathbf{k}} \hat{b}_{\mathbf{k}} + \sum_{\mathbf{k}\neq 0} V_{\mathbf{k}} e^{i\mathbf{k}\cdot\hat{\mathbf{r}}} \left(\hat{b}_{\mathbf{k}} + \hat{b}^{\dagger}_{-\mathbf{k}}\right), \tag{2}$$

given by the sum of the kinetic energy of the impurity particle with mass m_I, the energy of the phonons in the medium with dispersion $\omega_{\mathbf{k}}$, and the interaction energy with coupling constant $V_{\mathbf{k}}$ arising between the two of them. The coupling strength is essentially determined by the dielectric constant of the crystal and can be quantified by a single, dimensionless coupling constant α. The regime of small α is characterized by weak and intermediate polaron coupling while for values of $\alpha \gg 1$ the strong coupling regime is realized. Simple perturbation theory predicts the crossover around a value of $\alpha \approx 6$. Experimentally, Fröhlich polarons have been observed in condensed matter systems for small and moderate interaction strengths α, however, the regime of so-called strong coupled polarons with $\alpha \gg 1$ has so far not been experimentally investigated [25, 26].

Recently, the quantum gas Bose-polaron was subject of intense theoretical work. It was shown that the description of a Bose-polaron Eq. (1) can be directly mapped onto the Fröhlich Hamiltonian Eq. (2) via a Bogoliubov transform [6] and that this model could be accessed experimentally [7, 21]. This analogy holds as long as interaction effects within the BEC can be neglected, such as interaction of BEC excitations with each other [7, 21] or Efimov correlations [10]. The resulting Hamiltonian has the same operator structure as Eq. (2), where the crystal (optical) phonons are replaced by elementary Bogoliubov excitations of the BEC with dispersion $\varepsilon_{\mathbf{q}} = \hbar v_s q \sqrt{1 + (\xi q)^2/2}$, where $v_s = \hbar/(\sqrt{2} m \xi)$ is the sound

velocity in the BEC, $\xi = 1/\sqrt{8\pi n_{\mathrm{BEC}} a_{\mathrm{BB}}}$ is the healing length, n_{BEC} is the BEC atomic density, and a_{BB} is the s-wave scattering length between two atoms in the BEC. The polaronic coupling parameter in the dilute quantum gas scenario [6, 7]

$$\alpha = \frac{a_{\mathrm{IB}}^2}{a_{\mathrm{BB}}\xi} \tag{3}$$

is given by the s-wave scattering lengths between a Boson of the quantum gas with the impurity (a_{IB}) or with other quantum gas atoms (a_{BB}), and the condensate healing length ξ. For the quantum gas Bose-polaron, these parameters can be varied over a large range of values from the weakly interacting to the strong coupling regime by means of Feshbach resonances. In contrast to condensed matter systems, this allows for a systematic study of the polaronic features' dependence on the coupling strength. Characteristic properties of the emerging polaron are its binding energy E_{p} and its effective mass m_{p}. Both can be inferred similarly to recent studies in imbalanced ultracold Fermi mixtures by applying radio frequency spectroscopy [27–30], and trap frequency measurements [31], respectively. Importantly, also the Bose polaron beyond the Fröhlich model can be experimentally realized yielding access to a rich and highly controllable model system of impurity physics in quantum fluids.

2 Experimental realization

Our experimental approach to realizing the Bose polaron aims at immersing single or few neutral Caesium (^{133}Cs) atoms into a Rubidium (^{87}Rb) BEC. Using single impurities allows us to study the dynamics and properties of individual polarons. This is in contrast to solid-state systems, where only averaged polaronic effects can be measured by probing macroscopic properties of the material [25, 32]. While for single impurities polaron-polaron interaction effects [33] are absent, we can study these effects by choosing a specific number of multiple impurities. Moreover, tight external control over individual impurities allows to prepare and study polaron dynamics in steady state or in non-equilibrium states, which is challenging in typical condensed matter systems. Our combination of species features several advantages, facilitating the realization, control and characterization of the Bose polaron. First, due to the relatively high nuclear charge of Rb and Cs the fine structure splitting of both species is also relatively large and allows to tune dipole traps in between the two fine structure lines of the first excited P-level with moderate unwanted photon scattering [34, 35]. As a consequence the atoms of this element do not experience a dipole potential. In order to improve the control over both species independently, we employ this fact constructing a species-selective conveyor-belt lattice allowing for trapping and controlled transport of impurity atoms, only. The lattice offers a unique way to study nonequilibrium phenomena, such as polaron transport [36], coherence properties [17], or Bloch oscillations [37], being inaccessible in solid state systems.

Second, for a dipole trap wavelength of λ = 1,064 nm, the trapping frequency ω and thus the gravitational sag g/ω^2 with g the gravitational acceleration, is equal to the percent level for the two species. Therefore, a high spatial overlap is ensured when both species are trapped in the same dipole potential, even for ultracold temperatures. Third, with Cs representing the minority component, three-body losses limiting the lifetime of the polaron are due to Rb-Rb-Cs collisions rather than Cs-Cs-Rb collision, where the loss coefficient

L_3 of the former is an order of magnitude smaller than for the latter [38]. While three-body losses will still be a limitation of the atomic lifetime, the lifetime of the polaron is expected to be significantly larger than the lifetime in balanced Rb-Cs mixtures. Furthermore, fluorescence imaging of such a small number of atoms in an optical lattice allows for single-site resolved detection of the impurities with standard optical systems [39], enabling the tracking of single impurity dynamics with high precision.

For the design of the experimental apparatus, additional considerations have to be made. In a combined system of quantum gas and single atoms, the respective ways to experimentally extract information from averages differ: For a quantum gas, a single realization yields an ensemble average of typically $10^3 \ldots 10^5$ atoms. For single atoms, in contrast, averages have to be formed as time averages of typically $10^2 \ldots 10^3$ repetitions for identical parameter values. For a combination, the statistics is clearly limited by probing the single impurity, while usually the time scale of a single experimental run is limited by the production of a BEC. Therefore we produce a BEC all-optically in a crossed dipole trap with high trap frequencies, resulting in cycling times smaller than 7 seconds.

Our system therefore combines several advantages over previous experiments [38], such as spatial control and high resolution imaging of the impurity atoms combined with a short cycle time which enables us to study polaronic effects in yet unexplored regimes. In the following we first discuss the experimentally relevant parameter ranges and constraints for our system of single Cs impurities in a Rb BEC, before we turn to the presentation of our experimental apparatus.

2.1 The Rb-Cs Bose-polaron

For the experimental characterization of the Bose-polaron, we focus on the binding energy $E_\mathrm{p} = h\nu_\mathrm{p}$ in the following. This energy can be measured by radio or microwave spectroscopy, driving a Zeeman or hyperfine transition between two impurity states, where one state is interacting with the bosonic bath forming the polaron, whereas the other state is non-interacting or only weakly interacting. The polaron binding energy manifests itself as a shift of the transition's RF spectrum compared to an impurity without the bosonic bath, similar to Fermi-polarons [28, 29].

The method of RF spectroscopy is a standard tool for high-precision, but it is limited by the lifetime of the polaron. In our system the polaron decays predominantly by three-body losses, i.e. molecule formation, occurring with rate $\gamma_\mathrm{p} = n_\mathrm{BEC}^2 L_3$ with the loss coefficient L_3 and the BEC density n_BEC. The decay limits the time during which the rf transition occurs to $\tau = \frac{1}{\gamma_\mathrm{p}}$, implying a lower bound for the linewidth of the measured polaron spectroscopy peak. In order to clearly resolve the polaron peak at a frequency shift of ν_p, the ratio $\beta = \nu_\mathrm{p}/\gamma_\mathrm{p}$ should be significantly larger than 1 yielding a figure of merit for the determination of optimum experimental parameters.

In Figure 1 we explore the regimes of Bose polarons realized with our typical experimental parameters discussed below, employing theoretical data of elastic scattering length a_IB and three-body loss coefficient L_3 around the interspecies Feshbach resonance at 181 G [40]. The range of polaronic coupling strengths α accessible with our experimental setup is determined by several parameters: the boson-boson scattering length $a_\mathrm{BB} \approx 100 a_0$ [41], with the Bohr radius $a_0 = 53$ pm, is given by the background scattering length of Rb and does not change within the range of magnetic field values considered here; BEC peak densities are on the order of $n_\mathrm{BEC,max} = 10^{14}$ cm^{-3} which serves as a worst case approximation

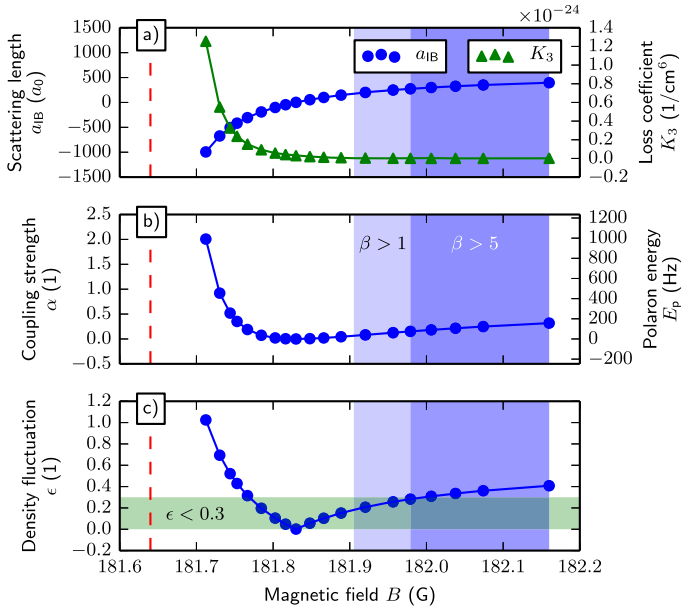

Figure 1 Bose polaron properties at the Feshbach resonance. (a) shows the theoretical values of the interspecies scattering length a_{IB} and the three-body loss coefficient K_3 for Rb-Rb-Cs scattering at the 181 G Feshbach resonance (dashed red). For our typical BEC density of 10^{14} cm^{-3} the estimated coupling strength α and the corresponding polaron energy E_p is shown in **(b)**. The vertical blue shaded area indicates fulfillment of the condition $\beta = \nu_p/\gamma_p > 5$ (>1 light shaded). **(c)** The parameter ϵ is derived in [7] and gives an estimate of how well the Bose polaron fits the Fröhlich type. The horizontal green shaded area indicates $\epsilon < 0.3$ which means good correspondence to the Fröhlich type polaron.

for n_{BEC}; and the interspecies scattering length $a_{IB} \approx 650 a_0$ at zero magnetic field is tunable in the vicinity of the Feshbach resonance [42, 43].

From this we calculate the polaron coupling constant α and polaronic binding energy E_p using a simple analytic expression for an impurity with infinite mass from [21], see Figure 1(b). Furthermore, the polaronic decay rate γ_p is calculated from the BEC peak density and theoretical values for L_3 in vicinity of the Feshbach resonance [40]. For $\beta > 1$, we can reliably resolve polarons spectroscopically within the discussed parameter ranges, indicated by the vertical shaded regions in Figure 1.

Furthermore, we use the parameter $\epsilon = 2\pi^{3/2}(1 + m_B/m_I)a_{IB}\sqrt{a_{BB}n_{BEC}}$ from [7] in Figure 1(c) to indicate where the Bose polaron realized can be described by means of the Fröhlich model discussed above, where $\epsilon \ll 1$ corresponds to a good description. One can see that ϵ lies well below 1 for the experimentally directly accessible range (blue), placing our setup mainly in the weak and intermediate coupling regime. For reference, the value of $\epsilon < 0.3$ given in [7] is marked as horizontally shaded area in Figure 1.

In conclusion, realizing a Bose-polaron is well possible with our experimental setup. Also the regime of Fröhlich-type polarons in the weak and intermediate coupling regime is well accessible and new polaron physics can be explored. For the observation of a strongly coupled Fröhlich polaron, the regime of $\beta > 1$ can be expanded towards higher a_{IB}, by lowering the 3-body lossrate. This can be achieved by reducing the BEC density, and thus decreasing ϵ, too, for example by increasing the trapping volume and levitating magnetically [44]. Employing Feshbach resonances with more favorable three-body loss properties, or the application of optical tuning methods [45] are being considered.

2.2 Rb Bose-Einstein condensate

In order to optimize the statistics of single atom probing, the experimental setup aims at a short BEC production time. This is realized by, first, a short initial laser cooling stage, where a 3D magneto-optical trap (MOT) is loaded from a 2D MOT in ≈2.5 s at a rate of 10^9 atoms/s and, second, evaporation in a steep optical dipole trap which is formed by a horizontal and a vertical beam within ≈4 s. In order to avoid perturbation from cooling and trapping of single Cs atoms in a MOT, the Rb cloud is prepared in the magnetic field insensitive $F = 1, m_F = 0$ state while evaporating. We typically prepare a BEC with 2.5×10^4 atoms at a peak density of 1.2×10^{14} cm^{-3} and a critical temperature of approximately 120 nK. The BEC's decay rate of 0.4 Hz is dominated by two- and three-body collisions at this density but decreases to 0.08 Hz for a lower number of atoms. For technical details of the BEC production and state preparation, see Section 3.

2.3 Single atoms

Single or few Cs atoms are captured in a high magnetic field gradient (≈250 G/cm) MOT [46], spatially overlapped with the Rb MOT, but operated at a different time in the preparation sequence. In contrast to the Rb MOT, the Cs MOT is loading atoms from the background, and the laser cooling beams have a smaller diameter and beam intensity, leading to an overall reduced loading rate. The fluorescence signal of such a MOT features discrete values, which can be assigned to a specific number of atoms in the MOT. A Poissonian distribution describes the loading statistics in the few atom regime, observed in a histogram of measured fluorescence signal, corresponding to the distribution of atom numbers in Figure 2(b). The width of each histogram peak is ideally given by the shot noise of the atoms' fluorescence light; practically, however, fluctuations of the MOT laser beam intensities and technical contributions such as readout noise additionally broaden the peaks. This limits the maximum countable atom number to roughly eight for our setup. Refer to Section 3 for technical details and a description of the fluorescence imaging system.

In order to provide position control over the single Cs atoms independently from the Rb BEC trap, we apply a species selective optical conveyor belt lattice, formed by two counter propagating, linearly polarized laser beams with wavelength $\lambda_{\text{lat}} = 790$ nm and a waist of 29 μm. For this wavelength between the Rb D-Lines, the resulting potential cancels out for Rb atoms [34, 35], but at the same time the frequency is blue detuned for Cs, providing confinement along the lattice axis in the nodes of the standing wave with depths up to $7{,}300 E_r^{\text{Cs}} = 850\ \mu\text{K} \times \text{k}_\text{B}$, with $E_r^{\text{Cs}} = \hbar^2 k^2 / 2 m_{\text{Cs}}$ the single photon recoil energy, $k = 2\pi/\lambda_{\text{lat}}$, k_B the Boltzmann constant, and m_{Cs} the mass of a Cs atom. While the lattice provides tight axial confinement for Cs atoms, it does not confine the atoms radially. We therefore superpose the lattice axis with one beam of the dipole trap (see Section 3) and obtain a maximum trap depth of 1.45 mK radially, resulting in trap frequencies of $2\pi \times 4$ kHz radially and $2\pi \times 460$ kHz axially. The lifetime of atoms in the lattice at full depth is limited to $\tau \approx 1.24$ s by phase fluctuations. If in addition an optical molasses is used to cool the atoms, the lifetime can be extended up to $\tau = 71$ s, limited by background pressure.

An important quantity characterizing the lattice is the selectivity $s = E_r^{\text{Rb}} / E_r^{\text{Cs}}$ for a given intensity and wavelength. By performing Raman-Nath [47–49] scattering on the BEC for various lattice wavelengths, we have identified the optimal wavelength around 780 nm and find a selectivity of 5,000 : 1 for Cs. In order to transport the Cs atoms by a defined

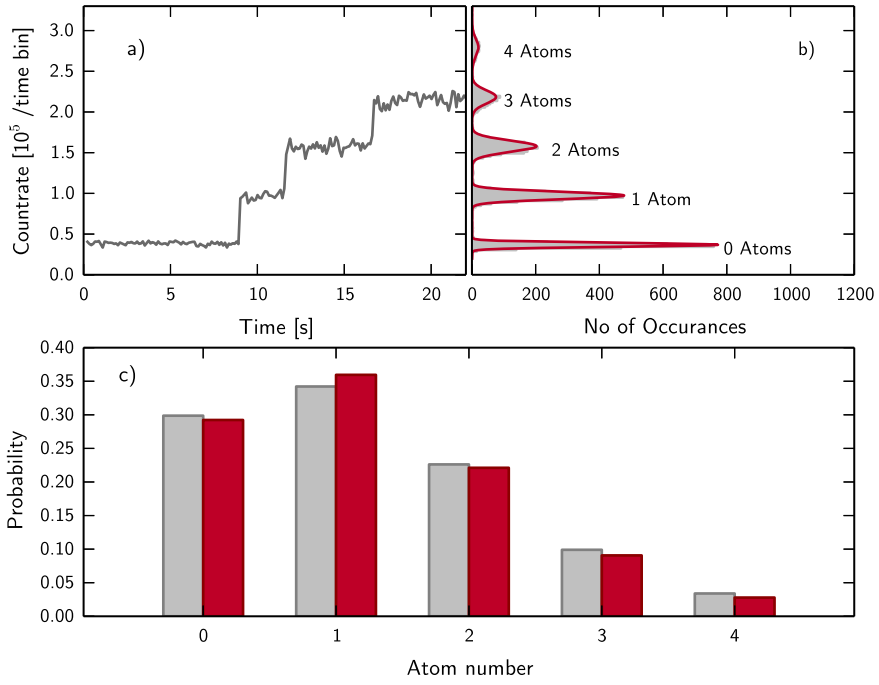

Figure 2 Loading curve and histogram of the high gradient MOT. (a) Typical loading trace of the single atom MOT. After 8 s a first atom is loaded into the MOT and in steps of 3-5 s an atom is gained. The time is binned in 110 ms to collect enough fluorescence photons. **(b)** Histogram of the electron count rate taken over 30 traces with 267 data points each. The red solid line shows a Multi-Gaussian fit to the data. **(c)** Probabilities for each atom number obtained from the area of each peak in the multi-Gaussian fit (gray bars) and from a Poisson distribution (red bars) with mean atom number $n = 1.23$, calculated from the histogram.

distance, a precisely controlled relative detuning δ between the lattice beams is used, which causes the standing wave interference pattern to move at a velocity $v = \lambda_{\text{lat}}\delta/2$ for a specific amount of time [50]. For details also see Section 3.

2.4 Combining single atoms with the quantum gas

During evaporation, the Rb cloud is prepared in the magnetic field insensitive state $|F = 1, m_F = 0\rangle$ by a radio frequency transition, see Section 3. After it has been sufficiently cooled down to be well localized in the dipole trap crossing region, the Cs MOT is switched on. To avoid immediate losses of the single Cs atoms due to light-induced collisions [51–53], both species are trapped in different traps with a displacement of 110 μm. Figure 3 shows the probability of Cs atoms surviving a 1.3 s MOT period while a cold thermal Rb cloud is present in the dipole trap crossing region in dependence of the crossing region's position. The minimum in survival probability marks the position of maximum overlap between MOT and dipole trap.

As an initial step towards immersing the Cs atoms into the Rb BEC, we immerse them into a thermal Rb gas. Here, the horizontal dipole trap is sufficiently deep to directly trap Cs atoms from the MOT. After switching off the Cs MOT, we let the two species interact for a certain time before pushing Rb out of the trap by shining in resonant light perpendicular to both dipole trap beams. The high gradient MOT is switched on to recapture the Cs atoms from the dipole trap and the number of atoms in both MOT phases is compared to each other. Figure 4 shows a measurement of the survival probability in dependence of

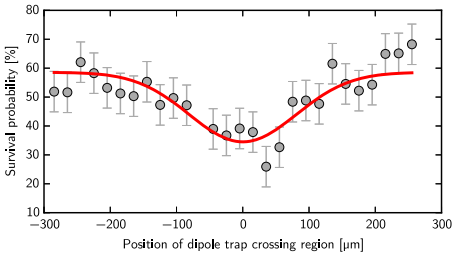

Figure 3 Light assisted collisions. The graph shows the probability of Cs atoms surviving a 1.3 s MOT period while a cold Rb cloud is present in the dipole trap crossing region in dependence of the crossing region's position along the horizontal dipole trap beam. We attribute the losses to light assisted collisions of Cs with Rb in the presence of near resonant Cs MOT light. A negative Gaussian fit (red) serves as a guide to the eye.

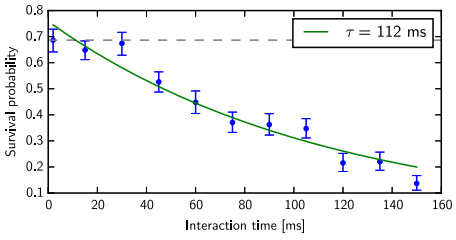

Figure 4 Lifetime of Cs in presence of a cold Rb cloud. The graph shows the probability of recapturing Cs atoms from the dipole trap after they have been stored together with a cold Rb cloud for a given 'interaction time'. Without Rb present in the trap, the survival probability is 0.69 (dashed gray). For a Rb cloud in $|F=1,m_F=0\rangle$ with 38,000 atoms at a temperature of $T=3\ \mu$K at trap frequencies of $\omega = 2\pi \times (63,1{,}300,1{,}300)$ Hz and a peak density of $\rho_0 = 1.3\times10^{13}$ cm^{-3}, the fit reveals a lifetime of $\tau = 112$ ms for Cs atoms in $|F=3\rangle$.

the time between switching off the Cs MOT and pushing out the Rb, which we refer to as 'interaction time'. For a Rb cloud in $|F=1,m_F=0\rangle$ with 38×10^3 atoms at a temperature of $T=3\ \mu$K at trap frequencies of $\omega = 2\pi \times (63,1{,}300,1{,}300)$ Hz and a peak density of $\rho_0 = 1.3\times10^{13}$ cm^{-3}, we measure a lifetime of $\tau = 112$ ms for Cs atoms in $|F=3\rangle$. We attribute the limited lifetime to two-body losses due to the fact that Rb and Cs have not been pumped to their lowest Zeeman states. For experiments in which Cs lifetime is crucial, we will pump Cs to $|F=3,m_F=3\rangle$ and Rb to $|F=1,m_F=1\rangle$, such that the lifetime is limited by 3-body losses with a loss coefficient of $L_3 = 5\times10^{-26}$ cm^{6}s^{-1} [38]. Here, the lifetime would be $\tau = \frac{1}{L_3}\langle n_{\mathrm{Rb}}^2\rangle = 608$ ms in the spin polarized case. For the relevant parameter range of $\beta > 1$ close to the Feshbach resonance shown in Figure 1, the lifetime is bounded above 74 ms…135 ms allowing to spectroscopically measure the polaron energy.

We see that the overlap in occupied trap volume of the two species decreases upon further cooling of the Rb cloud, leading to an increasing chance that the two species do not interact. For experiments involving colder Rb clouds, especially a BEC, the experiment will therefore be enhanced by an intermediate cooling step for Cs.

3 Methods

Our experiments take place in a two-chamber vacuum system consisting of a low pressure (≈10^{-10} mbar) and a high pressure region (≈10^{-7} mbar), separated by a differential pumping section of length 83 mm and diameter increasing from 1.8 mm to 4 mm. The low pressure region is formed by a glass cell, whereas the high pressure region is located in a titanium chamber and contains a 2D MOT for ^{87}Rb which is loading atoms from the background gas. The distance between the 3D MOT region and the 2D MOT is approximately 30 cm.

The coil system shown in Figure 5(b) is installed at the low pressure side, providing a quadrupole field for the Cs and Rb MOTs, a homogeneous field to address Feshbach resonances, and a vertical magnetic field gradient for Stern-Gerlach experiments. Addi-

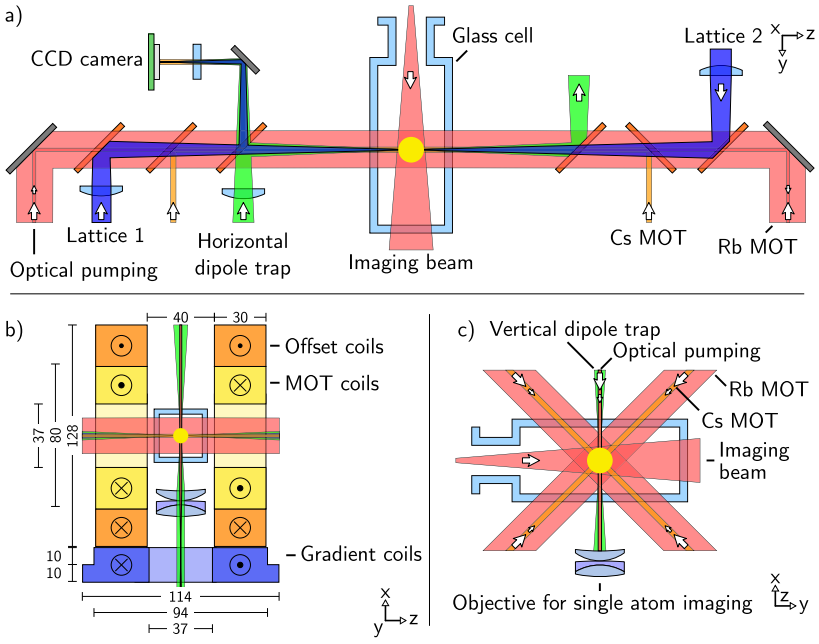

Figure 5 Overview of the experimental setup. (a) Experiment in top view: With dichroic mirrors beams for the optical dipole trap, MOTs for each species, the optical lattice for Cs, and an optical pumping beam for Rb are overlapped. A CCD camera resembles the position of the cold atoms which is useful for the initial alignment of the dipole trap and the optical lattice to the position of the Cs MOT. **(b)** Front view with main magnetic coils (dimensions in mm). **(c)** Side view.

tionally, compensation coils are installed to provide weak, homogeneous fields in all three dimensions up to 2 G to compensate magnetic stray fields.

Single atom MOT

The position of the Cs MOT is overlapped with the Rb MOT as both use the same coil system. A set of 6 diaphragms with variable aperture mounted in the coil holders is used to align the MOT beams to precisely overlap in the middle of the glass cell. The cooling light is 10 MHz red detuned to the $F = 4 \rightarrow F' = 5$ transition of the Cs D2 line and has a total power of typically 500 μW. The repumping light is on resonance to the $F = 3 \rightarrow F' = 3$ transition with a total power of typically 15 μW. In every beam pair a piezo driven mirror at 110 Hz frequency destroys phase coherence between orthogonal beam pairs and therefore avoids interference effects, which lead to an instable MOT position. To keep the MOT loading time short, a low magnetic field gradient of 40 G/cm axially and 20 G/cm radially is applied for 20 ms. During this sufficiently short time the trap volume is large enough to load on average one atom [54]. In a next step the magnetic field gradient is increased in 8 ms to 275 G/cm in axial and 140 G/cm in radial direction. This effectively pins the atom number and avoids additional atom loading during the imaging process. The duration of the low gradient stage depends on the vapor pressure of the Cs atoms and the required atom number. For an efficient transfer of the trapped atoms into the optical dipole trap, a low MOT temperature is needed. Therefore we increase the red detuning of the cooler light to 72 MHz for 50 ms, while setting its power so low that we just do not lose the atoms. We release the atoms into the dipole trap by switching off the MOT beams. The cooler

is switched off 2 ms after the repumper ensuring that the atoms remain in their lowest fine-structure state $|F = 3\rangle$.

Optical dipole trap and evaporative cooling

Our BEC is produced in a crossed beam optical dipole trap at 1,064 nm. The trap is formed by a horizontal beam with a focal waist of $w_0 = 22\ \mu$m at 4 W and a vertical beam with a focal waist of $w_0 = 165\ \mu$m at 12 W of power, yielding trap frequencies of 3.7 kHz radial to the horizontal beam and 120 Hz along the horizontal beam. The beam setup allows both for a forced evaporation scheme [55] as well as standard, passive evaporation [56]. The laser light is generated by a Nufern NUA-1064-PD-0050-D0 fiber amplifier and transported to the experiment by two optical fibers (LMA-PM-15 by NKT Photonics and Liekki Passive-10/125-PM). A PID controller and AOMs are employed to stabilize the dipole trap beams' power with a bandwidth of 110 kHz.

After the Rb MOT has been loaded, both dipole trap beams are switched on at full power during a CMOT phase [57, 58]. The repumping light is switched off 200 μs before the cooling light, so that Rb is pumped to the $F = 1$ state and approx. 10^6 atoms are transferred to the dipole trap. After 300 ms of self-evaporation we decrease the horizontal beam's power exponentially. As soon as the increase in density within the crossing region causes atom loss, we ramp down the power of the vertical beam as well until a BEC with 2.5×10^4 atoms forms after a total evaporation time of 4.3 s. The entire BEC sequence, including 3D MOT loading, CMOT phase and evaporation ramps has been optimized with an evolutionary algorithm, that is implemented as a part of our timing software [59].

Internal state preparation

The Rb atoms are prepared in the magnetically insensitive state $|F = 1, m_F = 0\rangle$ during evaporation so that the magnetic field gradient of the single atom MOT does neither heat nor destroy the cold Rb cloud: During self-evaporation, a magnetic field of 1.4 G is switched on to lift the degeneracy of the Zeeman substates. Then the atoms are pumped to the $|F = 1, m_F = 1\rangle$ state by a 900 μs light pulse resonant to the $F = 1 \rightarrow F' = 1\ \sigma^+$-transition and a 500 μs light pulse resonant to the $F = 2 \rightarrow F' = 2\ \pi$-transition of the D_2 line. Both beams are turned on simultaneously. Their respective powers are 300 nW and 480 μW with red detunings of 2.6 MHz and 1 MHz at equal beam waists of 1.2 mm.

By applying a magnetic field gradient of typically 5.7 G/cm during a 13 ms time of flight experiment, we perform a Stern-Gerlach experiment to measure the population of magnetic substates. Without optical pumping we observe an almost equally distributed spin mixture, while with optical pumping approximately 90% of the atoms are in the $m_F = 1$ Zeeman substate and approximately 10% remain in $m_F = 0$. Optical pumping does not deplete the number of atoms in the condensate.

After optical pumping we transfer the population to the $m_F = 0$ state with a Landau-Zener sweep: We apply a radio frequency at 10.176 MHz for 100 ms while we increase the magnetic field linearly. The magnetic field ramp is chosen such that the detuning of the radio frequency with respect to the $|m_F = 1\rangle \rightarrow |m_F = 0\rangle$ transition falls from approximately +550 kHz to −550 kHz. We observe a Rabi-frequency of $\Omega = 2\pi \times 2.1$ kHz with a transfer efficiency of 95%, with no negative impact on the number of atoms in the BEC.

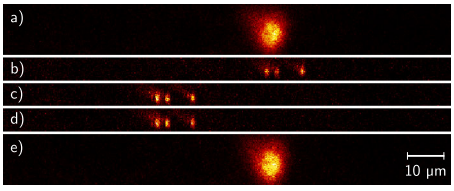

Figure 6 Fluorescense images of single Cs atoms in MOT and lattice. Four consecutive images of three single Cs atoms. **(a)** Fluorescence image of Cs atoms trapped in a MOT, **(b)** after being transferred to the species-selective conveyor belt lattice, **(c)** after being moved for 30 µm, **(d)** after being held in place, **(e)** after being transferred back to the MOT.

3.1 Single atom imaging

To observe the single atoms we use fluorescence imaging. Near resonant light from the MOT beams is scattered in the whole solid angle. We collect 3.3% of the photons corresponding to 0.012 pW/atom for a saturation parameter $S_0 = I/I_s = 1$ by a custom made objective. It has a numerical aperture (NA) of 0.36 and is placed beneath the glass cell at a distance of 30.3 mm to the atoms' position (see Figure 5(c)). Stray light protection is crucial and the whole beam path is located inside black anodized lens tubes and mirror housings.

The objective tube is mounted on a precision xyz linear stage (Newport Ultralign Model 562-XYZ) for accurate positioning. The light which is collimated by the objective is focused onto an EMCCD camera (Andor iXon 3 897) by a lens with focal length $f = 1{,}000$ mm. This yields a magnification of $M = 33$. The camera chip has 512×512 pixel with a pixel size of 16×16 μm which leads to a field of view of 250 μm. An advantage of this setup is that the objective can be aligned independently from the focusing lens which is producing the image on the camera. The high EMCCD gain and the quantum efficiency of nearly 60% of the camera allows to observe single atoms in the MOT as well as in the optical lattice (see Figure 6). During imaging the atoms are illuminated by the repumper light of the MOT and cooler light, which is 20 MHz red detuned in order to compensate the light shift caused by the dipole trap. Exposure times of 150 ms (400 ms) in the MOT (lattice) are usually used to image the atoms. The number of atoms in the MOT can be determined with close to 100% reliability from the brightness of the image.

3.2 Optical lattice

Our optical lattice consists of a two beam setup (see Figure 5), where both beams are guided to the experiment by means of optical fibers with identical length. This helps to reduce phase drifts and guarantees a good beam quality at the experimental side. To make sure that the lattice beams and the horizontal dipole trap beam are overlapped with each other and hit the small-volume Cs MOT, we exploit the AC stark effect. The lattice frequency is blue detuned and hence enhances the fluorescence of the MOT, whereas the dipole trap is red detuned and reduces the fluorescence (see Figure 7).

3.3 Lattice transport

For the single atom transport in the conveyor belt optical lattice [50], a relative detuning δ between the two lattice beams is employed to create a standing wave pattern, moving at velocity $v = \lambda_{\mathrm{lat}}\delta/2$. For a typical transport, the detuning between the beams is ramped in a trapezoid shape: a linear ramp from zero to the maximum detuning yields an acceleration of the atoms in the lattice, followed by a plateau of constant detuning where the atoms move at constant velocity. After this plateau, the detuning is ramped back to zero and the atoms are decelerated again. The transport distance is given by the integral over the velocity. Thereby large transport distances in the range of millimeters can be realized, which are

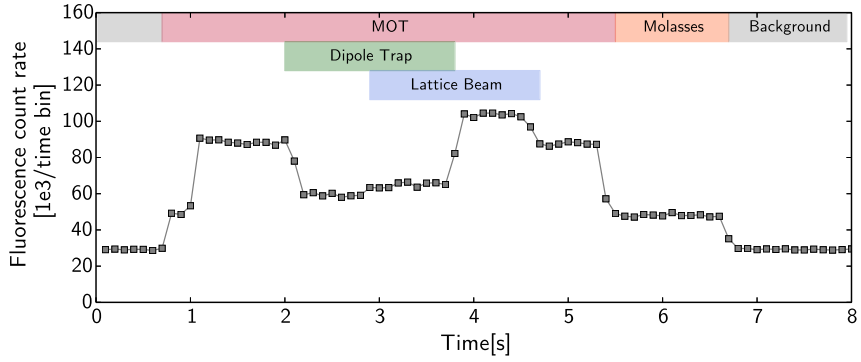

Figure 7 AC Stark effect of dipole trap and lattice. A typical fluorescence trace with lattice and dipole trap beam. During the MOT phase one atom is captured. Switching on the dipole trap reduces the fluorescence level by about 70%. In combination with the lattice a slight increase is observed because it compensates the light shift of the dipole trap. For the combination of MOT and lattice an increase of about 10% in fluorescence level is observed. In the end the count rate due to stray light and the dark count rate is detected. A binning time of 100 ms is used.

only limited by trap size. This is in contrast to phase shifting transport approaches, where the maximum transport distance is given by the maximum phase shift [60]. The absolute maximum acceleration $a_{\max} = kU_0/m_{\mathrm{Cs}} \approx 4 \cdot 10^5$ m/s^2 in the lattice is determined by the Cs mass m_{Cs}, the laser wave number k and the potential depth $U_0 \approx 1.5$ mK of the standing wave potential.

In order to control the detuning, each lattice beam is frequency shifted by a common value of $f_1 \approx f_2 = 160$ MHz in an AOM double-pass setup. The relative detuning between the two beams then is given by $\delta = f_1 - f_2$ and can be controlled by the two RF frequencies supplied to the AOMs. Both RF signals have to be phase-stable compared to each other and the offset-frequency of both channels has to be equal up to a fraction of a Hertz to yield a stable standing wave pattern when both beams interfere for $\delta = 0$ Hz. Therefore, we use a driver electronics based on direct digital synthesis ('DDS') with an amplifier chain. The DDS chips employed (AD9954) sample the output sine wave in a digital circuit and have an analog digital converter stage for signal output. By supplying both DDS chips with the same clock signal which is locked to a Rb frequency standard, the relative phase stability between the signals is guaranteed by the digital sampling of the output signal. The frequency of the output sine wave is set by a 32 bit control parameter, yielding a frequency resolution of 0.09 Hz which allows for very small frequency variations compared to the output frequency of 80 MHz. To supply output powers of up to ∼30 dBm a two stage amplifier chain combined with a voltage controlled attenuator for output power control is applied. The RF power level can be directly used to adjust and stabilize the light intensity of the lattice beams. The DDS chips are controlled by a microcontroller which provides exact timing of frequency changes and stores the data for the frequency ramps.

4 Conclusion

We have presented a cold gas experimental system to study the Bose polaron by immersion of single neutral Cs impurities into a Rb BEC. This single-impurity approach yields the possibility of investigating individual polarons in a highly controlled system. By tuning the impurity-bath interaction, a wide range of coupling strengths from the weak to

the strong coupling regime is accessible. We have estimated typical parameters, characterizing Fröhlich-type Bose-Polarons in our system. Our estimations show the feasibility of spectroscopically measuring the binding energy of Fröhlich-polarons in the weak and intermediate coupling regime with our current setup and how the strong coupling regime can be reached. With an all-optical approach to BEC production, we reach short cycle times needed to obtain good statistics for single-impurity measurements. Experimentally, we have demonstrated trapping and transporting of impurity atoms in a species-selective conveyor-belt lattice, as well as imaging with high optical resolution. Furthermore, we have shown the successful immersion of single impurities into a cold gas and their detection after a defined interaction time. The combination of high-resolution imaging and position control in a quantum gas will allow a systematic study of static and dynamical properties of individual polarons as well as interaction effects of multi-polaron systems.

Competing interests
The authors declare that they have no competing interests.

Author's contributions
All authors contributed in the design, build-up and characterization of the experiment, as well as the writing of this manuscript. All authors read and approved the final manuscript.

Author details
[1] Department of Physics and Research Center OPTIMAS, University of Kaiserslautern, Gottlieb-Daimler-Strasse 47, Kaiserslautern, 67663, Germany. [2] Graduate School Materials Science in Mainz, Gottlieb-Daimler-Strasse 47, Kaiserslautern, 67663, Germany.

Acknowledgements
The project was financially supported partially by the European Union via the ERC Starting Grant 278208 and partially by the DFG via SFB/TR49. D.M. is a recipient of a DFG-fellowship through the Excellence Initiative by the Graduate School Materials Science in Mainz (GSC 266), F.S. acknowledges funding by Studienstiftung des deutschen Volkes, and T.L. acknowledges funding from Carl-Zeiss Stiftung.

Received: 30 July 2015 Accepted: 30 October 2015 Published online: 14 November 2015

References

1. Ng HT, Bose S. Single-atom-aided probe of the decoherence of a Bose-Einstein condensate. Phys Rev A. 2008;78:023610. doi:10.1103/PhysRevA.78.023610.
2. Daley AJ, Fedichev PO, Zoller P. Single-atom cooling by superfluid immersion: a nondestructive method for qubits. Phys Rev A. 2004;69:022306. doi:10.1103/PhysRevA.69.022306.
3. Griessner A, Daley AJ, Clark SR, Jaksch D, Zoller P. Dark-state cooling of atoms by superfluid immersion. Phys Rev Lett. 2006;97:220403. doi:10.1103/PhysRevLett.97.220403.
4. Klein A, Fleischhauer M. Interaction of impurity atoms in Bose-Einstein condensates. Phys Rev A. 2005;71:033605. doi:10.1103/PhysRevA.71.033605.
5. Cucchietti FM, Timmermans E. Strong-coupling polarons in dilute gas Bose-Einstein condensates. Phys Rev Lett. 2006;96:210401. doi:10.1103/PhysRevLett.96.210401.
6. Tempere J, Casteels W, Oberthaler MK, Knoop S, Timmermans E, Devreese JT. Feynman path-integral treatment of the BEC-impurity polaron. Phys Rev B. 2009;80:184504. doi:10.1103/PhysRevB.80.184504.
7. Grusdt F, Shchadilova YE, Rubtsov AN, Demler E. Renormalization group approach to the Fröhlich polaron model: application to impurity-BEC problem. Sci Rep. 2015;5:12124.
8. Klein A, Bruderer M, Clark SR, Jaksch D. Dynamics, dephasing and clustering of impurity atoms in Bose-Einstein condensates. New J Phys. 2007;9:411. doi:10.1088/1367-2630/9/11/411.
9. Christensen RS, Levinsen J, Bruun GM. Quasiparticle properties of a mobile impurity in a Bose-Einstein condensate. arXiv:1503.06979 (2015).
10. Levinsen J, Parish MM, Bruun GM. Impurity in a Bose-Einstein condensate and the Efimov effect. Phys Rev Lett. 2015;115:125302. doi:10.1103/PhysRevLett.115.125302.
11. Ardila LAPN, Giorgini S. Impurity in a Bose-Einstein condensate: study of the attractive and repulsive branch using quantum Monte Carlo methods. Phys Rev A. 2015;92:033612. doi:10.1103/PhysRevA.92.033612.
12. Yin T, Cocks D, Hofstetter W. Polaronic effects in one- and two-band quantum systems. arXiv:1509.08283 (2015).
13. Grusdt F. An all-coupling theory for the Fröhlich polaron. arXiv:1509.08974 (2015).
14. Palzer S, Zipkes C, Sias C, Köhl M. Quantum transport through a Tonks-Girardeau gas. Phys Rev Lett. 2009;103:150601. doi:10.1103/PhysRevLett.103.150601.
15. Fukuhara T, Kantian A, Endres M, Cheneau M, Schauß P, Hild S, Bellem D, Schollwöck U, Giamarchi T, Gross C, Bloch I, Kuhr S. Quantum dynamics of a mobile spin impurity. Nature. 2009;9:235-41. doi:10.1038/nphys2561.
16. Ospelkaus S, Ospelkaus C, Wille O, Succo M, Ernst P, Sengstock K, Bongs K. Localization of bosonic atoms by fermionic impurities in a three-dimensional optical lattice. Phys Rev Lett. 2006;96:180403. doi:10.1103/PhysRevLett.96.180403.

17. Scelle R, Rentrop T, Trautmann A, Schuster T, Oberthaler MK. Motional coherence of fermions immersed in a Bose gas. Phys Rev Lett. 2013;111:070401. doi:10.1103/PhysRevLett.111.070401.
18. Zipkes C, Palzer S, Sias C, Köhl M. A trapped single ion inside a Bose-Einstein condensate. Nature. 2010;464:388-91. doi:10.1038/nature08865.
19. Schmid S, Härter A, Hecker Denschlag J. Dynamics of a cold trapped ion in a Bose-Einstein condensate. Phys Rev Lett. 2010;105:133202. doi:10.1103/PhysRevLett.105.133202.
20. Balewski JB, Krupp AT, Gaj A, Peter D, Büchler HP, Löw R, Hofferberth S, Pfau T. Coupling a single electron to a Bose-Einstein condensate. Nature. 2013;502:664-7. doi:10.1038/nature12592.
21. Shashi A, Grusdt F, Abanin DA, Demler E. Radio-frequency spectroscopy of polarons in ultracold Bose gases. Phys Rev A. 2014;89:053617. doi:10.1103/PhysRevA.89.053617.
22. Landau LD. Phys Z Sowjetunion. 1933;3:664.
23. Pekar SI. Research in electron theory of crystals. Moscow: Gostekhizdat; 1951.
24. Fröhlich H. Electrons in lattice fields. Adv Phys. 1954;3(11):325-61. doi:10.1080/00018735400101213.
25. Hodby JW. Cyclotron resonance of the polaron in the alkali and silver halides - observation of the dependence of the effective mass of the polaron on its translational energy. Solid State Commun. 1969;7(11):811-4. doi:10.1016/0038-1098(69)90767-4.
26. Madelung O, Rössler U, Schulz M, editors. Indium antimonide (InSb), conduction band, effective masses. In: Group IV elements, IV-IV and III-V compounds. Part b - electronic, transport, optical and other properties. Berlin: Springer; 2002. p. 1-10. (Landolt-Börnstein - group III condensed matter; vol 41A1b). doi:10.1007/10832182-371.
27. Schunck CH, Shin Y, Schirotzek A, Zwierlein MW, Ketterle W. Pairing without superfluidity: the ground state of an imbalanced Fermi mixture. Science. 2007;316(5826):867-70. doi:10.1126/science.1140749.
28. Schirotzek A, Wu C-H, Sommer A, Zwierlein MW. Observation of Fermi polarons in a tunable Fermi liquid of ultracold atoms. Phys Rev Lett. 2009;102:230402. doi:10.1103/PhysRevLett.102.230402.
29. Kohstall C, Zaccanti M, Jag M, Trenkwalder A, Massignan P, Bruun GM, Schreck F, Grimm R. Metastability and coherence of repulsive polarons in a strongly interacting Fermi mixture. Nature. 2012;485(7400):615-8.
30. Koschorreck M, Pertot D, Vogt E, Frohlich B, Feld M, Kohl M. Attractive and repulsive Fermi polarons in two dimensions. Nature. 2012;485(7400):619-22.
31. Nascimbène S, Navon N, Jiang KJ, Tarruell L, Teichmann M, McKeever J, Chevy F, Salomon C. Collective oscillations of an imbalanced Fermi gas: axial compression modes and polaron effective mass. Phys Rev Lett. 2009;103(17):170402. doi:10.1103/PhysRevLett.103.170402.
32. Miyake SJ. Strong-coupling limit of the polaron ground state. J Phys Soc Jpn. 1975;38(1):181-2. doi:10.1143/JPSJ.38.181.
33. Casteels W, Tempere J, Devreese JT. Bipolarons and multipolarons consisting of impurity atoms in a Bose-Einstein condensate. Phys Rev A. 2013;88(1):013613. doi:10.1103/PhysRevA.88.013613.
34. LeBlanc LJ, Thywissen JH. Species-specific optical lattices. Phys Rev A. 2007;75:053612. doi:10.1103/PhysRevA.75.053612.
35. Arora B, Sahoo BK. State-insensitive trapping of Rb atoms: linearly versus circularly polarized light. Phys Rev A. 2012;86:033416. doi:10.1103/PhysRevA.86.033416.
36. Bruderer M, Klein A, Clark SR, Jaksch D. Transport of strong-coupling polarons in optical lattices. New J Phys. 2008;10(3):033015. doi:10.1088/1367-2630/10/3/033015.
37. Grusdt F, Shashi A, Abanin D, Demler E. Bloch oscillations of bosonic lattice polarons. Phys Rev A. 2014;90:063610. doi:10.1103/PhysRevA.90.063610.
38. Spethmann N, Kindermann F, John S, Weber C, Meschede D, Widera A. Dynamics of single neutral impurity atoms immersed in an ultracold gas. Phys Rev Lett. 2012;109:235301. doi:10.1103/PhysRevLett.109.235301.
39. Karski M, Förster L, Choi JM, Alt W, Widera A, Meschede D. Nearest-neighbor detection of atoms in a 1D optical lattice by fluorescence imaging. Phys Rev Lett. 2009;102:053001. doi:10.1103/PhysRevLett.102.053001.
40. Wang Y. Private communication (2012).
41. van Kempen EGM, Kokkelmans SJJMF, Heinzen DJ, Verhaar BJ. Interisotope determination of ultracold rubidium interactions from three high-precision experiments. Phys Rev Lett. 2002;88:093201. doi:10.1103/PhysRevLett.88.093201.
42. Pilch K, Lange AD, Prantner A, Kerner G, Ferlaino F, Nägerl H-C, Grimm R. Observation of interspecies Feshbach resonances in an ultracold Rb-Cs mixture. Phys Rev A. 2009;79:042718. doi:10.1103/PhysRevA.79.042718.
43. Takekoshi T, Debatin M, Rameshan R, Ferlaino F, Grimm R, Nägerl H-C, Le Sueur CR, Hutson JM, Julienne PS, Kotochigova S, Tiemann E. Towards the production of ultracold ground-state RbCs molecules: Feshbach resonances, weakly bound states, and the coupled-channel model. Phys Rev A. 2012;85:032506. doi:10.1103/PhysRevA.85.032506.
44. Lercher AD, Takekoshi T, Debatin M, Schuster B, Rameshan R, Ferlaino F, Grimm R, Nägerl H-C. Production of a dual-species Bose-Einstein condensate of Rb and Cs atoms. Eur Phys J D. 2011;65(1-2):3-9. doi:10.1140/epjd/e2011-20015-6.
45. Compagno E, De Chiara G, Angelakis DG, Palma GM. Tunable polarons in Bose-Einstein condensates. arXiv:1410.8833 (2014).
46. Haubrich D, Schadwinkel H. Observation of individual neutral atoms in magnetic and magneto-optical traps. Europhys Lett. 1996;34:663-8.
47. Martin PJ, Oldaker BG, Miklich AH, Pritchard DE. Bragg scattering of atoms from a standing light wave. Phys Rev Lett. 1988;60:515-8. doi:10.1103/PhysRevLett.60.515.
48. Cahn SB, Kumarakrishnan A, Shim U, Sleator T, Berman PR, Dubetsky B. Time-domain de Broglie wave interferometry. Phys Rev Lett. 1997;79:784-7. doi:10.1103/PhysRevLett.79.784.
49. Gadway B, Pertot D, Reimann R, Cohen MG, Schneble D. Analysis of Kapitza-Dirac diffraction patterns beyond the Raman-Nath regime. Opt Express. 2009;17(21):19173-80. doi:10.1364/OE.17.019173.
50. Kuhr S, Alt W, Schrader D, Dotsenko I, Miroshnychenko Y, Rosenfeld W, Khudaverdyan M, Gomer V, Rauschenbeutel A, Meschede D. Coherence properties and quantum state transportation in an optical conveyor belt. Phys Rev Lett. 2003;91:213002. doi:10.1103/PhysRevLett.91.213002.
51. Spethmann N, Kindermann F, John S, Weber C, Meschede D, Widera A. Inserting single Cs atoms into an ultracold Rb gas. Appl Phys B. 2012;106:513-9.

52. Weber C, John S, Spethmann N, Meschede D, Widera A. Single Cs atoms as collisional probes in a large Rb magneto-optical trap. Phys Rev A. 2010;82:042722. doi:10.1103/PhysRevA.82.042722.
53. Weiner J, Bagnato VS, Zilio S, Julienne PS. Experiments and theory in cold and ultracold collisions. Rev Mod Phys. 1999;71:1-85. doi:10.1103/RevModPhys.71.1.
54. Kuhr S. A controlled quantum system of individual neutral atoms. PhD thesis. Bonn; 2003.
55. Clément J-F, Brantut J-P, Robert-de-Saint-Vincent M, Nyman RA, Aspect A, Bourdel T, Bouyer P. All-optical runaway evaporation to Bose-Einstein condensation. Phys Rev A. 2009;79:061406. doi:10.1103/PhysRevA.79.061406.
56. Arnold KJ, Barrett MD. All-optical Bose-Einstein condensation in a 1.06 μm dipole trap. Opt Commun. 2011;284:3288-91.
57. Ketterle W, Davis KB, Joffe MA, Martin A, Pritchard DE. High densities of cold atoms in a dark spontaneous-force optical trap. Phys Rev Lett. 1993;70:2253-6. doi:10.1103/PhysRevLett.70.2253.
58. Lewandowski HJ, Harber DM, Whitaker DL, Cornell EA. Simplified system for creating a Bose-Einstein condensate. J Low Temp Phys. 2003;132(5-6):309-67.
59. Lausch T, et al. Paper in preparation.
60. Belmechri N, Förster L, Alt W, Widera A, Meschede D, Alberti A. Microwave control of atomic motional states in a spin-dependent optical lattice. J Phys, At Mol Opt Phys. 2013;46:104006. doi:10.1088/0953-4075/46/10/104006.